Ultrasonics - Sonochemistry 69 (2020) 105238

Contents lists available at ScienceDirect

Ultrasonics - Sonochemistry

journal homepage: www.elsevier.com/locate/ultson

Does power ultrasound (26 kHz) affect the hydrogen evolution reaction (HER) on Pt polycrystalline electrode in a mild acidic electrolyte?

Bruno G. Pollet[a,*], Faranak Foroughi[a], Alaa Y. Faid[b], David R. Emberson[c], Md.H. Islam[a]

[a] Hydrogen Energy and Sonochemistry Research Group, Department of Energy and Process Engineering, Faculty of Engineering, Norwegian University of Science and Technology (NTNU), NO-7491 Trondheim, Norway

[b] Electrochemistry Research Group, Department of Materials Science and Engineering, Faculty of Natural Sciences. Norwegian University of Science and Technology (NTNU), NO-7491 Trondheim, Norway

[c] Combustion Kinetics Group, Department of Energy and Process Engineering, Faculty of Engineering, Norwegian University of Science and Technology (NTNU), NO-7491 Trondheim, Norway

ARTICLE INFO

Keywords:
Ultrasound
Sonoelectrochemistry
Hydrogen evolution reaction
Platinum
Bubble overpotential

ABSTRACT

In this study, we investigated the effects of power ultrasound (26 kHz, up to ~75 W/cm^2, up to 100% acoustic amplitude, ultrasonic horn) on the hydrogen evolution reaction (HER) on a platinum (Pt) polycrystalline disc electrode in 0.5 M H_2SO_4 by cyclic and linear sweep voltammetry at 298 K. We also studied the formation of molecular hydrogen (H_2) bubbles on a Pt wire in the absence and presence of power ultrasound using ultra-fast camera imaging. It was found that ultrasound significantly increases currents towards the HER i.e. a ~250% increase in current density was achieved at maximum ultrasonic power. The potential at a current density of −10 mA/cm^2 under *silent* conditions was found to be −46 mV and decreased to −27 mV at 100% acoustic amplitude i.e. a ΔE shift of ~ +20 mV, indicating the influence of ultrasound on improving the HER activity. A nearly 100% increase in the exchange current density (j_o) and a 30% decrease in the Tafel slope (b) at maximum ultrasonic power, was observed in the low overpotential region, although in the high overpotential region, the Tafel slopes (b) were not significantly affected when compared to *silent* conditions. In our conditions, ultrasound did not greatly affect the "real" surface area (A_r) and roughness factor (R) i.e. the microscopic surface area available for electron transfer. Overall, it was found that ultrasound did not dramatically change the mechanism of HER but instead, increased currents at the Pt surface area through effective hydrogen bubble removal.

1. Introduction

Electrochemical water splitting technologies for hydrogen generation will play a key role in meeting climate change targets [1]. Currently, ca. 4% of the global hydrogen production is produced through water electrolysis using water electrolysers, whilst 96% is produced through Steam Methane Reforming (SMR) [2]. Electrochemical water splitting is a process in which, a direct current (DC) is passed through two electrodes in an aqueous solution by applying a cell voltage (V_{cell}), whereby di-oxygen (O_2) and di-hydrogen (H_2) gases are generated at the anode and cathode respectively [3–11].

Based upon the type of electrolytes, separators, working temperatures and pressures employed, there are currently four water electrolyser technologies, namely: (i) Alkaline Water Electrolyser (AWE, aqueous KOH or NaOH, NiO, < 80 °C, < 30 bar), (ii) Proton Exchange Membrane Water Electrolyser (PEMWE, liquid water, perfluorosulfonic acid (PFSA), < 80 °C, < 200 bar), (iii) Solid Oxide Electrolyser Cell (SOEC, water steam, yttrium-stabilized zirconia (YSZ), 500–850 °C, atmospheric), and (iv) Molten Carbonate Electrolyser (MCE, molten sodium and potassium carbonate, 600–700 °C, 1–8 bar) [3–6].

PEMWEs and AWEs are the most commercially available and used electrolysers for producing "green" hydrogen, as they both offer many advantages such as: well-established technologies, ease of use, compact system design, quick response, high dynamic operations, high current densities, greater H_2 production rate of acceptable purity (99.99%) and fairly high energy efficient (80–90% for PEMWE and 70–80% for AWE) [10]. However, they both suffer from molecular hydrogen and oxygen bubble accumulation at the electrode surfaces and in the electrolyte, leading to a high ohmic voltage drop (IR) and a large reaction overpotential (η), in turn yielding high operational energy consumption and costs [12,13].

Unfortunately, H_2 and O_2 gas bubble evolutions during electrochemical water splitting are unavoidable phenomenon yielding electrochemical losses. This is due to the fact that the electrochemical

* Corresponding author.
E-mail address: bruno.g.pollet@ntnu.no (B.G. Pollet).

https://doi.org/10.1016/j.ultsonch.2020.105238
Received 10 May 2020; Received in revised form 17 June 2020; Accepted 22 June 2020
Available online 26 June 2020

reaction rates for both reactions are purely controlled by the interfacial phenomenon in the three-phase zone (TPZ) where H_2 and O_2 gas bubbles, electrolyte and electrode surface are in contact with each other [13].

V_{cell} for electrochemical water splitting technologies is shown in equation (1) [3,4].

$$V_{cell} = |Ec - Ea| + I \times \sum R = E\text{rev} + |\eta_a| + |\eta_c| + I \times (R_c + R_m + R_b + R_e) \quad (1)$$

where E_c (or E_{HER}) is the cathode potential for the hydrogen evolution reaction (HER), E_a (or E_{OER}) is the anode potential for the oxygen evolution reaction (OER), I is the applied current, $\sum R$ is total ohmic resistance, E^{rev} is the reversible potential (*Nernst*), η_a is the anode overpotential, η_c is the cathode overpotential, R_c is the circuit resistance, R_m is the membrane/separator resistance, R_b is the bubble resistance, and R_e is the electrolyte resistance [12].

Equation (1) shows that V_{cell} is greatly dependent upon the overpotential and ohmic voltage drop and therefore, minimizing η_a, η_c and $\sum R$ is paramount to minimise energy consumption. During water electrolysis, R_c and R_m are usually constant and can be reduced by better wire connection and membrane (or separator) optimisation. However, it is not the situation for R_b as many evolved gas bubbles generated on the electrode surface act as a "passivation layer" i.e. an insulating layer, which significantly reduces the effective electrode surface area (A_{eff}). In this case, the bubble coverage (Θ) on the electrode surface leads to increased bubble resistance, R_b. This fraction of the electrode surface covered with "sticking" gas bubbles is well-known to affect substantially: (i) the mass (m) and heat (h) transfer, (ii) the limiting current density (j_{lim}), (iii) the overpotential (η) and (iv) $\sum R$. In other words, when the evolved gas bubbles cover the electrode surface, they cause electrolyte access blockage and yield reactant starvation resulting to an exponential increase of V_{cell} with the current density (j). Additonally, the dispersion of the bubbles in the electrolyte decreases its conductivity and in turns increases R_e and thus, the current distribution on the electrode surface increases yielding high cell voltages [12–18].

In a typical low-tempearture water electrolyser, V_{cell} is ca. 1.8 – 2.0 V at an operating current density of ca. 100 – 300 mA/cm^2, a value which is much higher than the theoretical cell voltage of 1.229 V, yielding a ($\Sigma\eta + \Sigma R$) of ca. + 571 – +771 mV, mainly caused by H_2 and O_2 gas evolution processes. The gas bubbles should therefore be removed from the TBZ as rapidly as possible. There are several methods for reducing the total overpotential and total ohmic resistance in water electrolysis, for example, by either increasing the electrolyte flowrate, by using gravity, or by using a magnetic field on the gas-evolving electrodes [12,13].

Another method is to apply power ultrasound. Power ultrasound (PUS) is a well-defined sound wave in the range 20 kHz – 2 MHz (10 – 1,000 W/cm^2) and it is regarded as the effect of the sound wave on the medium. It is now well-known that PUS used in electrochemistry causes: (a) an area of intense mixing at the vicinity of the ultrasonic transducer, (b) electrolyte degassing, (c) electrode surface activation, cleaning and erosion, (d) an increase in electrolyte bulk temperature, (e) cavitation, (f) sonolysis (i.e. the production of highly reactive radicals) and (g) sono(electrochemi)luminescence [19–24].

In 2011, it was observed by Pollet and co-workers at the *Birmingham PEM Fuel Cell research group* that PUS could efficiently remove molecular hydrogen and oxygen bubbles from the electrolyte and electrode surfaces in turn enhancing hydrogen and oxygen electrochemical production rates [25–27]. Lepesant [25] and other researchers such as Symes [26] and Zadeh [27,28] from the same research group, studied the effects of PUS on the sonoelectrolytic (20 kHz) hydrogen production from mild acidic and alkaline electrolytes on various electrode material types. They observed that PUS increased the hydrogen and oxygen production rates due to the efficient electrode cleaning, and electrode surface/solution degassing and enhanced mass transfer of electroactive species to the electrode surface. Recently Islam *et al.* [29] reviewed the area in a paper entitled "sonochemical and sonoelectrochemical production of hydrogen" and showed that PUS can be a powerful tool to overcome the limitations of electrochemical water splitting technologies for hydrogen production via: (i) electrode surface cleaning and activation, (ii) increased mass transfer in the bulk electrolyte and near the electrode surface, and (iii) efficient degassing at the electrode surface and electrolyte. They also showed that PUS can improve the electrolytic efficiency (up to 60%) caused by increased ion concentration and bubble removal at the electrode surface [29].

There are only a few reports in the literature dealing with the effects of PUS on the HER (and OER). For example, Banerjee *et al.* [30] found that the ultrasonication (25 kHz, 250 W) of aqueous mixtures consisting of Zn particles and $NiCl_2$ in HCl enhanced hydrogen evolution due to reduced mass transfer contribution yielding an ohmically controlled process. Walton *et al.* [31] showed that ultrasound (38 kHz) slightly affects the HER from 1.0 M H_2SO_4 at platinised platinum electrode due to improved removal of adherent product species on the electrode surface. McMurray *et al.* [32] demonstrated that the HER and OER are affected by ultrasound (20 kHz, 26 W/cm^2) on a titanium sonotrode (the vibrating ultrasonic horn acting as the working electrode) immersed in a neutral aqueous electrolyte (0.7 M Na_2SO_4 adjusted to pH7 using 0.1 M NaOH), and concluded that these observations were mainly due to enhanced mass transport as well as increased metallic corrosion rates induced by intense agitation and cavitation at the electrode surface. S.D. Li *et al.* [33] and J. Li *et al.* [34] investigated the effects of power ultrasound (25.3 kHz, 33.3 kHz, 60 kHz, < 50 W) on a Pt electrode immersed in mild alkaline solutions (0.1 M, 0.5 M and 1.0 M NaOH). They found that ultrasound helped in removing the thin layer of bubbles at the electrode surface, especially at lower concentrations. Lin and Hourng [35] showed by the aid of electrochemical impedance spectroscopy (EIS) that ultrasound (113 kHz, up to 900 W) improved the activity and concentration impedances and greatly improved the removal of hydrogen bubbles at the electrode surface and in the electrolyte. Since the bubble surface coverage (Θ) is proportional to the ohmic resistance (R) and overall cell overpotential [36], then PUS should, in theory, reduce V_{cell} [12].

However, in these studies, in-depth kinetic analyses were not undertaken in order to shed some light on the effects of ultrasound on the HER mechanisms and Tafel parameters in mild acidic and alkaline electrolytes. The kinetics of the fundamental HER reactions (as well as the hydrogen oxidation reaction - HOR, oxygen reduction reaction ORR and oxygen evolution reaction - OER) are simply based upon "microkinetic analyses" and can be described by: (a) the dependence of the Tafel slope on the coverage of the formed surface species, e.g. M − H for the HER/HOR, M − OH, M − O, M − OOH and M − OO − for the ORR/OER, where M is the electrode surface site, and (b) the Butler-Volmer equation in explaining electrocatalytic kinetics [37].

Theoretically, simple electrochemical redox reactions can be described by the Butler-Volmer equation (BVE) shown in Equation (2) [37].

$$j = j_0 \left\{ \exp\left((1-\alpha)\frac{zF}{RT}\eta \right) - \exp\left[-\alpha\frac{zF}{RT}\eta \right] \right\} \quad (2)$$

where η is the overpotential, which is the difference between the electrode applied (E_{app}) and reversible potentials (E^{rev}) ($\eta = E_{app} - E^{rev}$), j is the current density (A/m^2), α is the transfer coefficient, z is the number of electrons transferred, F is the Faraday constant (96,489C/mol), R is the universal gas constant (8.314 J/mol/K), T is the absolute temperature (K), and j_o is the exchange current density (A/m^2). The equation represents the total currents from both the reduction and oxidation reactions. Experimentally, two limiting forms of the BVE are used to obtain the Tafel equations [37].

At large positive overpotentials, i.e. when $\eta \rightarrow +\infty$ i.e.

$\exp\left[\left(\frac{-\alpha zF}{RT}\right)\eta\right] \rightarrow 0$, then the BVE can be approximated to:

$$j = j_0\left\{exp\left[\left((1-\alpha)\frac{zF}{RT}\right)\eta\right]\right\} \quad (3)$$

or

$$\log(j) = \log(j_0) + \frac{(1-\alpha)zF}{(2.303RT)}\eta \quad (4)$$

or

$$\eta = -2.303\frac{RT}{(1-\alpha)zF}\log(j_0) + 2.303\frac{RT}{(1-\alpha)zF}\log(j) \quad (5)$$

At large negative overpotentials, i.e. $\eta \rightarrow -\infty$, the BVE can be approximated to:

$$j = -j_0\left\{exp\left[\left((-\alpha)\frac{zF}{RT}\right)\eta\right]\right\} \quad (6)$$

or

$$\log(|j|) = \log(j_0) - \frac{\alpha zF}{(2.303RT)}\eta \quad (7)$$

or

$$\eta = 2.303\frac{RT}{\alpha zF}\log(j_0) - 2.303\frac{RT}{\alpha zF}\log(|j|) \quad (8)$$

The logarithmic relationships are known as the Tafel equations in the form of:

$$\eta = a + b\log(j) \quad (9)$$

where

$$a = -2.303\frac{RT}{(1-\alpha)zF}\log(j_0) \text{ for when } \eta \rightarrow +\infty \quad (10)$$

or

$$a = +2.303\frac{RT}{\alpha zF}\log(j_0) \text{ for when } \eta \rightarrow -\infty \quad (11)$$

and

$$b = +2.303\frac{RT}{(1-\alpha)zF} \text{ for when } \eta \rightarrow +\infty \quad (12)$$

or

$$b = -2.303\frac{RT}{\alpha zF} \text{ for when } \eta \rightarrow -\infty \quad (13)$$

The Tafel slope (b) provides insight into the reaction mechanism, and the exchange current density (j_o) are known as descriptors of the catalytic activity. Thus, for analysing electrochemical performances, the Tafel analysis is conjugated with the Butler-Volmer equation in many studies.

In the case of the HER, there are two general possible pathways [4,38]:

$$\text{In acidic electrolyte: } 2H^+ + 2e^- \rightarrow H_2(g) \quad E^o = 0.000\,\text{V vs. SHE.} \quad (14)$$

$$\text{In alkaline electrolyte: } 2H_2O(aq) + 2e^- \rightarrow H_2(g) + 2OH^-(aq)$$
$$E^{\varnothing} = -0.828\,\text{V vs. SHE} \quad (15)$$

Under Standard Temperature and Pressure (*STP*) i.e. $T = 298.15$ K and $P_{H2} = 1$ atm, the equilibrium or *Nernst* potential for the HER in acidic electrolyte is described by Equation (16):

$$E_{HER} = E^o_{H_2/H^+} + \frac{RT}{zF} \times \ln\left(\frac{P^{0.5}_{H_2}}{a_{H^+}}\right) = -0.059 \times pH \quad (16)$$

where E_{HER} is the *Nernst* potential (V vs. RHE), $E^o_{H_2/H^+}$ is the standard reduction potential for the redox couple H_2/H^+ (0.000 V vs. SHE), R is the ideal gas constant (8.3145 J/mol/k), T is the temperature (K), z is the number of electrons transferred, F is the Faraday constant (96,489C/mol), P_{H_2} is the hydrogen pressure (atm), and a_{H^+} is the activity of protons (mol/l).

There are three primary steps involved in the HER reaction in acidic media and each step has its characteristic Tafel slope value [38]:

$$H_3O^+ + e- \rightarrow H_{ads} + H_2O \text{ Volmer reaction: } b = 120\,\text{mV/dec} \quad (17)$$

$$H_{ads} + H_3O^+ + e- \rightarrow H_2 + H_2O \text{ Heyrovsky reaction: } b = 40\,\text{mV/dec} \quad (18)$$

$$H_{ads} + H_{ads} \rightarrow H_2 \text{ (chemical) Tafel reaction: } b = 30\,\text{mV/dec} \quad (19)$$

The first discharge step (Volmer reaction) is followed by either an electrochemical desorption step (Heyrovsky reaction) or a recombination step (Tafel reaction). The Tafel slope value is an inherent indicator of the electrocatalyst to show the rate-limiting step of the HER.

In this study, we investigated the effects of power ultrasound on the HER on Pt polycrystalline electrode in 0.5 M H_2SO_4 by cyclic and linear sweep voltammetry at 298 K. We also studied the formation of molecular hydrogen bubble in the absence and presence of power ultrasound using ultra-fast camera imaging.

2. Experimental methods

All electrochemical experiments were carried out using a potentiostat/galvanostat (BioLogic SP-150) in a 3-electrode configuration. In this study, two sonoelectrochemical cells were used as shown in Fig. 1(a) and Fig. 1(b).

All voltammetry work was performed using a specially designed sono-reactor placed in an *in-house* Faraday cage (Fig. 1(a)). This sono-reactor also called the *Besançon cell* has been fully characterized and well-described elsewhere [21,22,39]. The working electrode (WE) was either a polycrystalline platinum (Pt-poly) disc ($\varnothing$ = 0.182 cm) of geometric surface area (A_g) of 0.027 ± 0.002 cm^2 or a Pt-poly wire (L = 8 cm, $\varnothing$ = 0.1 cm). The reference electrode (RE) was a home-made reversible hydrogen electrode (RHE). The counter electrode (CE) was a Pt wire ($\varnothing$ = 0.5 mm, 99.95%, Alfa Aesar) sealed in a glass tube. The distance between the ultrasonic probe and the working electrode was ca. 3 cm. All working electrodes were electrochemically cleaned in sulfuric acid (1.0 mol/L) for 10 min prior to the experiments. They were then washed with ultrapure water (Millipore, 18.2 MΩ.cm). All 0.5 mol/L H_2SO_4 working electrolytes (pH = 0.3) were made from pure H_2SO_4 purchased from Merck (purity 96%). The temperature of the electrolyte was measured with a Fluke 51 digital thermometer fitted to a *K*-type thermocouple.

For all cyclic voltammetry (CV) and linear sweep voltammetry (LSV) experiments, the acquired potential values were modified by *IR* compensation correction based on the following equation:

$$E_{IRcorrected} = E - IR \quad (20)$$

where I is the measured current density and R the resistance of electrolyte, which was measured in 0.5 mol/L H_2SO_4 solution. The R value was determined by electrochemical impedance spectroscopy (EIS) from the value of the *real* impedance (Z) where the *imaginary* impedance (Z') is zero in Nyquist plot. The EIS experiments (not shown here) were carried out from 100 kHz to 0.01 Hz with a voltage perturbation of + 10 mV at an applied potential of −0.05 V vs. RHE and at T = 298 K [40].

The exchange current density (j_o) was obtained by the extrapolation method from the corresponding Tafel plot. According to Tafel equation: $\eta = a + b\log(j)$ (a and b are calculated from Tafel plot, see earlier), j_o can be obtained by extrapolating the Tafel plots to the x-axis or assuming η is zero [40–42].

The onset potentials (E_{onset}) at a current density of –1 mA/cm^2 and the potentials at a current density of –10 mA/cm^2 were obtained from the HER LSVs. Here, it should be emphasized that it is not a straightforward method to determine "precise" values. However in the

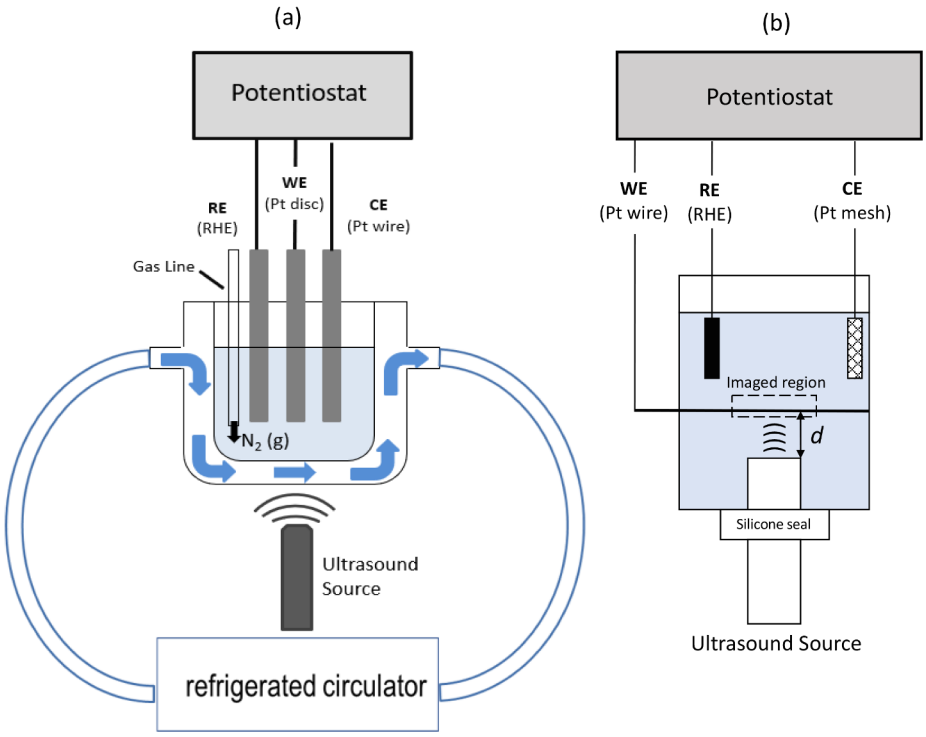

Fig. 1. (a) Sonoelectrochemical cell used for the voltammetry study; (b) Sonoelectrochemical cell used for high-speed imaging.

literature, the onset potential is usually calculated at a current density of –1 mA/cm^2 [40,42] and the potential value for a current density of –10 mA/cm^2 (i.e. the current density expected for a 12.3% efficient solar water-splitting device) is also regarded as another critical factor to assess HER activity [42,43]. In this study, we present both potential values i.e. at current densities of –1 mA/cm^2 ($E_{onset} = E_{-1mA/cm^2}$) and at –10 mA/cm^2 at (E_{-10mA/cm^2}).

For all sonoelectrochemical experiments, ultrasound was provided by a 26 kHz (f) ultrasonic probe (Hielscher UP200Ht, 200 W @ 100% fixed amplitude, tip ∅ = 7 mm, tip area = 38.48 mm^2 (3.85 × 10^{-3} cm^2). The ultrasonic or acoustic powers were determined calorimetrically using the methods of Margulis *et al.* [44] and Contamine *et al.* [45] and using Equation (21):

$$P_{acous} = (dT/dt)_{t=0} \times m \times C_p \quad (21)$$

where $(dT/dt)_{t=0}$ is the temperature slope per unit of ultrasonication time (at $t = 0$) in K/s; m is the mass of the water used in g and C_p is the specific heat capacity of water as 4.186 J/g/K. Here, the calorimetric method consists in measuring the heat dissipated in a known mass or volume of water, taking into account the water heat capacity (C_p) in which the acoustic energy is absorbed. This method assumes that all absorbed acoustic energy is transformed into heat. From the calorimetric experiments, the acoustic power, P_{acous} in W was determined. In our conditions, the acoustic power (P_{acous}) was found to be 4.65 W, 12.10 W, 18.30 W, 25.0 W and 29.20 W at 20%, 40%, 60%, 80% and 100% ultrasonic amplitude respectively.

All high-speed imaging water electrolysis experiments were performed in an *in-house* made perspex sonoelectrochemical cell – 50 mm × 50 mm × 150 mm with the ultrasonic horn inserted through the base and sealed with a silicon ring (Fig. 1(b)) using the sonoelectrochemical setup described in Fig. 2. A platinum (Pt) wire was used as the working electrode (WE) placed horizontally in the sonoelectrochemical cell with the electrical connections made external to the cell. The reference (RHE, RE) and counter electrodes (Pt wire, CE) were inserted into the corners of the sonoelectrochemical cell in a vertical orientation. High speed images were captured using a Photron SA 5 camera, at a frame rate of 10,000 frames per second (fps) using diffused back-lit illumination. The light source was a high power single chip LED (CBT 120) with light collimated onto an engineered diffusor (ThorlabsED1-C50) placed behind the sonoelectrochemical cell. A short exposure time of 1 ms was applied at a resolution of 896 × 848. The camera was fitted with a Nikon 60 micro lens and the resulting region that could be imaged was approx. 25 mm^2 and a record length of 2 s (see Fig. 1(b) and 2(b)). Prior to image collection, the ultrasonic probe was used to efficiently degas the solution to reduce imaging gas bubbles that were not associated with water electrolysis.

(a) Camera set-up: Camera Photron SA5 with a Nikon 60 mm Macro f2.8 lens. Maximum aperture used. Frame rate of 10,000 fps, 898 × 848 resolution, 33.26 µs exposure time, illuminated by a fibre optic illuminator (Cole Parmer Mod 41500–55). The light source was a high power single chip LED (CBT120) with light collimated onto an engineered diffusor (ThorlabsED1-C50) placed behind the sonoelectrochemical (SE) cell. (b) SE cell set up.

3. Results and discussion

3.1. Study of the underpotentially deposited hydrogen (UDH) in the absence and presence of ultrasound

3.1.1. Silent conditions

Fig. 3 shows a cyclic voltammogram (CV) of a polycrystalline Pt disc electrode in 0.5 M H_2SO_4 at a scan rate of 50 mV/s and at 298 K after purging with N_2(g) for 30 min. The CV profile exhibits the typical electrochemical features of a pure Pt-poly surface in which three regions ([i], [ii] and [iii]) can be clearly distinguished, namely:

(i) Regions [i] - The underpotentially deposited hydrogen (UPD-*H*) region (+0.05 – +0.45 V vs. RHE) where adsorption (H_{upd}, negative current densities) and desorption peaks (H_{upd}, positive current densities) for UPD-*H* are observed between + 0.05 and + 0.40 V vs. RHE. The two pairs of redox peaks are usually attributed to strongly and weakly adsorbed *H* atoms at the Pt surface, respectively.
(ii) Region [ii] - The capacitive double-layer region (+0.45 – +0.60 V

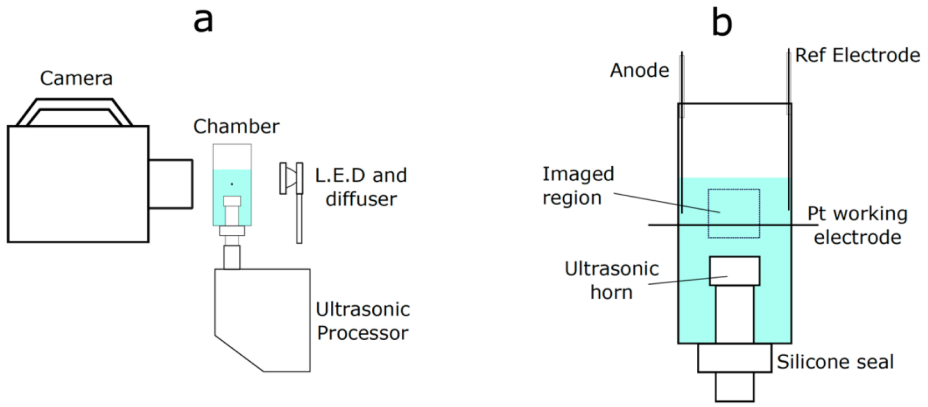

Fig. 2. Sonoelectrochemical setup for high-speed imaging.

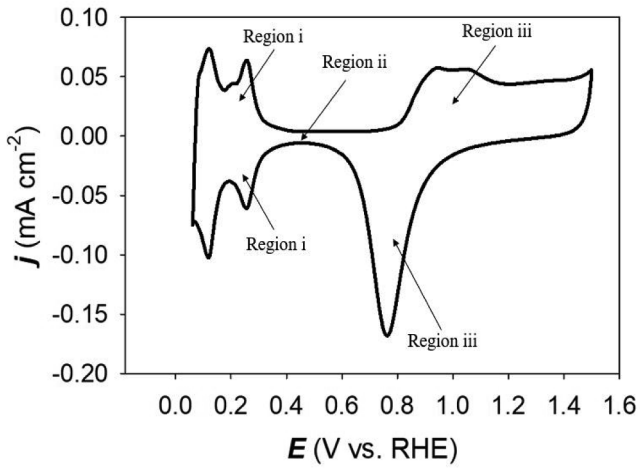

Fig. 3. A typical cyclic voltammogram of 0.5 M H_2SO_4 on a polycrystalline Pt disc electrode at a scan rate of 50 mV/s and at T = 298 K after purging with N_2(g) for 30 min.

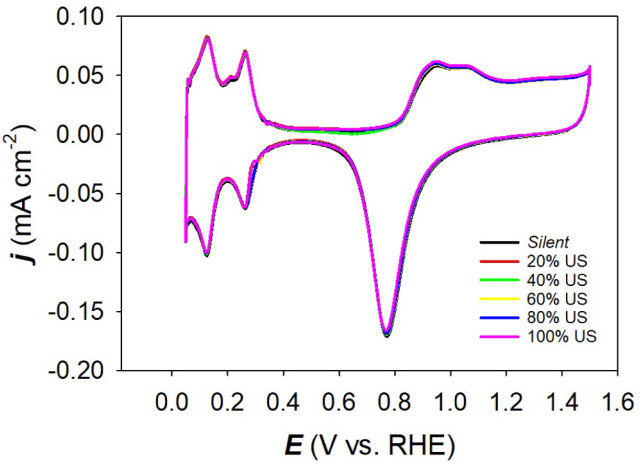

Fig. 4. A series of cyclic voltammograms (CVs) of 0.5 M H_2SO_4 on a polycrystalline Pt disc electrode at a scan rate of 50 mV/s and at T = 298 K after the Pt disc electrode was subjected to ultrasound (26 kHz) at various ultrasonic amplitudes (20%, 40%, 60%, 80% and 100%) for 6 min.

vs. RHE), in the centre of the CV, only represents capacitive processes [46].

(iii) Regions [iii] - The formation and reduction of Pt (hydr)oxide above + 0.60 V vs. RHE. This pair of redox peaks appears during the positive and negative scans, which is normally attributed to the formation (positive current densities) and reduction (negative current densities) of Pt hydroxide/oxide ($PtOH/PtO_x$) at the Pt electrode surface [46,47].

From the CV, the "real" surface area (A_r) of the Pt-poly electrode can be calculated by determining, after correction from the capacitive current density, the coulombic charge associated to the H_{upd} desorption in the + 0.05 to + 0.45 V vs. RHE potential region, according to Equation (22):

$$A_r = \frac{\frac{1}{v}\int i(E)\mathrm{d}E}{Q_{monolayer}} \quad (22)$$

where $i(E)$ is the current (μA) recorded at potential E (V vs. RHE) in the hydrogen desorption region, v is the linear potential variation or potential scan rate (V/s) and $Q_{monolayer}$ (μC/cm^2) is the coulombic charge related to the adsorption or desorption of a hydrogen monolayer on a polycrystalline Pt surface ($Q_{monolayer}$ = 210 μC/cm^2) [46,47]. A value of 0.037 ± 0.001 cm^2 for the A_r was obtained against 0.027 ± 0.002 cm^2 for the geometric surface area (A_g), e.g. a roughness factor (A_r/A_g) ≈ 1.38.

3.1.2. Ultrasonic conditions

Fig. 4 shows a series of cyclic voltammograms (CVs) of 0.5 mol/L H_2SO_4 on a polycrystalline Pt disc electrode at a scan rate of 50 mV/s and at 298 K after the Pt disc electrode was subjected to continuous ultrasonication (26 kHz) at various ultrasonic amplitudes (20%, 40%, 60%, 80% and 100%) for 6 min during the linear sweep voltammetry (LSV) experiments (see Fig. 5). For clarification, all CVs were performed just after each LSV experiment i.e. the Pt disc electrode was kept in the electrolyte that was subjected to sonication. Table 1 shows the coulombic charges associated to (i) the H_{upd} adsorption (Q_{ads}), (ii) the H_{upd} desorption (Q_{des}), (iii) the formed PtO (Q_{PtO}), (iv) the PtO reduction (Q'_{PtO}), as well as the double layer capacitance (C_{dl}), the "real" Pt electrode surface area (A_r) and the roughness factor (R) under *silent* and after ultrasonic conditions (26 kHz) at various ultrasonic powers and at 298 K, determined and calculated from Fig. 4 and Equation (22).

Fig. 4 and Table 1 clearly show that ultrasound does not have a significant effect on the shape of the CVs and the charges associated with Pt surface reaction in 0.5 mol/L H_2SO_4. These observations are in good agreement with those found by Walton *et al.* [31], although in their conditions, the CVs from 1 M H_2SO_4 at platinised platinum electrode were generated under continuous insonation (38 kHz, ultrasonic bath).

Table 1 shows that as the ultrasonic amplitude increases from 0 to 100%, Q_{ads}, Q_{des}, Q_{PtO}, and Q'_{PtO} slightly decrease. The decrease in these charges could be due to changes in electrode surface morphology due to the collapse of cavitation bubbles which could influence the adsorbate coverage on the electrode surface as previously observed by

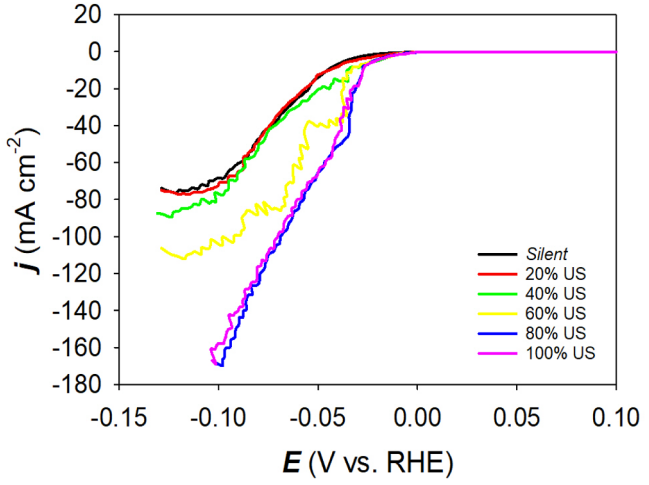

Fig. 5. Linear sweep voltammograms (LSVs) on 0.5 mol/L H_2SO_4 on a polycrystalline Pt disc electrode at a scan rate of 1 mV/s and at $T = 298$ K after purging with N_2(g) for 30 min under (a) *silent* and (b) ultrasonic conditions (26 kHz, ultrasonic amplitude: 20%, 40%, 60%, 80% and 100%).

Walton et *al.* [31].

For example, it can be observed that Q_{des} decreased from 294.88 μC/cm^2 to 279.99 μC/cm^2 as the ultrasonic amplitude was increased from 0 to 100% acoustic amplitude. However, the C_{dl} shows an adverse trend where C_{dl} increased from 219.69 μF/cm^2 to 249.98 μF/cm^2 as the acoutic amplitude increased from 0 to 100%. Similar observations were found by Zhang and Coury [48] who attributed this increase to an increased surface functionalisation (*pseudo-capacitance*) and slight changes in electrode surface area.

In our conditions, A_r and R i.e. the microscopic area available for electron transfer was not evidently affected by ultrasound for all acoustic powers used, indicating that the electrochemical surface area was not greatly modified due to erosion caused by the implosion of acoustic cavitation bubble on the electrode surface. For example, at maximum ultrasonic power, only a < 5% decrease in A_r and R was observed when compared to *silent* conditions (Table 1). These findings are in very good agreement with those observed by Zhang and Coury [48] as well as Pollet [49] who showed that the electrode surface area and roughness factor was little affected by ultrasound. In some instances, they found that a slight increase in electrode surface area was observed after prolonged sonication (5 min, 20 kHz, 475 W) due to electrode activation, through possible removal of adsorbed species on the electrode surface i.e. surface cleaning. Overall, no significant enhancements under insonation were observed.

3.2. Study of the effect of ultrasonic power on the hydrogen evolution reaction

Fig. 5 shows a series of LSVs on a Pt disc in 0.5 mol/L H_2SO_4 under *silent* and ultrasonic conditions up to 100% amplitude. To quantitatively compare the performance of an "ideal" HER (and OER) electrocatalyst, it should exhibit lower onset potentials and deliver higher current densities with lower overpotentials. From Table 1, it can be observed that the onset potentials gradually decreased from −17.6 mV vs. RHE under *silent* conditions to −5.7 mV vs. RHE at maximum ultrasonic power as the ultrasonic amplitude increased to 100% i.e. a ΔE shift of ~ +10 mV was achieved. It can also be noted that the potential at −10 mA/cm^2 under *silent* conditions was found to be −46 mV and decreased to −27 mV at 100% i.e. a ΔE shift of ~ +20 mV, indicating the influence of ultrasound on improving HER activity. The slopes of the LSV branches in the range [−0.05 V vs. RHE – −0.10 V vs. RHE] increased from 1.15 mA/cm^2/mV (*silent* conditions) to 1.93 mA/cm^2/mV (100% ultrasound), in other words, steeper LSV branches were obtained under sonication. Moreover, the current density at an electrode potential of −0.10 V vs. RHE increased as ultrasound amplitude increased from 0% (~70 mA/cm^2) to 100% (~170 mA/cm^2) i.e. a ~250% increase in current density was achieved at maximum ultrasonic power. It is worth noting that the LSVs at 0, 20, 40, and 60% ultrasonic amplitude exhibited "plateaux" at high current densities due to hydrogen bubble accumulation on the electrode surface while LSVs at 80% and 100% ultrasound showed straight LSV branches in the same high current density region, confirming bubble removal under intense agitation (see later). All sono-LSVs also exhibited, at high current densities, current spikes in the range of [-0.07 V vs. RHE - −0.14 V vs. RHE], due to both hydrogen bubble accumulation and cavitation bubbles imploding at the electrode surface. Birkin *et al.* [50] and recently Islam *et al.* [39] showed that the current spikes were mainly attributed to the implosion of cavitation bubbles at the electrode surface. Overall, the electrochemical conditions under 100% ultrasound amplitude led to improved and superior HER activity.

Fig. 6 shows the Tafel plots of Pt-poly disc under *silent* and ultrasonic conditions. Table 2 shows that the Pt disc exhibited fairly similar Tafel slopes under these conditions at low and high overpotential regions. At the low overpotential region, the Pt disc displays Tafel slopes of b ~ 20 – 30 mV/dec suggesting that the Tafel recombination reaction is the rate-determining step, following the fast initial Volmer discharge step. However, it is worth noting that the Tafel slope value at maximum ultrasonic power (b = 21 mV/dec) was much lower than that under *silent* conditions (b = 30 mV/dec) i.e. a ~ 30% decrease. As the overpotential is increased i.e. in the high overpotential region, the sonicated and non-sonicated Pt disc shows Tafel slopes of b ~ 120 mV/dec i.e. the coverage of absorbed hydrogen approaches saturation. This leads to an accelerated Tafel recombination step and the Volmer discharge step becomes the rate-determining step [37,47].

j_o is a key parameter to evaluate HER catalytic activity. Table 2 also shows that the j_o values for Pt disc under *silent* and ultrasonic conditions increased from + 0.27 to + 0.50 mA/cm^2 as the ultrasonic amplitude increased from 0 to 100%, in other words, a nearly 100% increase in j_o was observed under maximum ultrasonic conditions. As the j_o value is proportional to the electrochemical active surface area (ECSA) or A_r, this finding indicates high electrode catalytic activity, and thus rapid

Table 1
Coulombic charge associated to the H_{upd} adsorption (Q_{ads}), coulombic charge associated to the H_{upd} desorption (Q_{des}), coulombic charge associated to the formed PtO (Q_{PtO}), coulombic charge associated to the PtO reduction (Q'_{PtO}), double layer capacitance (C_{dl}), "real" Pt electrode surface area (A_r) and roughness factor (R) under *silent* and after ultrasonic conditions (26 kHz) at various ultrasonic powers and at 298 K.

Ultrasonic power, P_{acous} W (acoustic amplitude %)	Q_{ads} μC/cm^2	Q_{des} μC/cm^2	Q_{PtO} μC/cm^2	Q'_{PtO} μC/cm^2	C_{dl} μF/cm^2	A_r * cm^2	R
0 (*Silent*)	286.31	294.88	328.95	485.67	219.69	0.0374	1.38
4.65 (20)	273.51	284.88	322.28	456.26	226.32	0.0358	1.33
12.10 (40)	279.48	296.72	330.37	454.78	192.8	0.0370	1.37
18.30 (60)	285.86	284.11	326.04	482.66	227.42	0.0366	1.36
25.00 (80)	269.87	260.11	323.69	472.99	232.29	0.0340	1.26
29.20 (100)	278.61	279.99	328.40	463.20	249.98	0.0359	1.33

*Calculated from Equation (22) and using $Q_{monolayer}$ = 210 μC/cm^2.

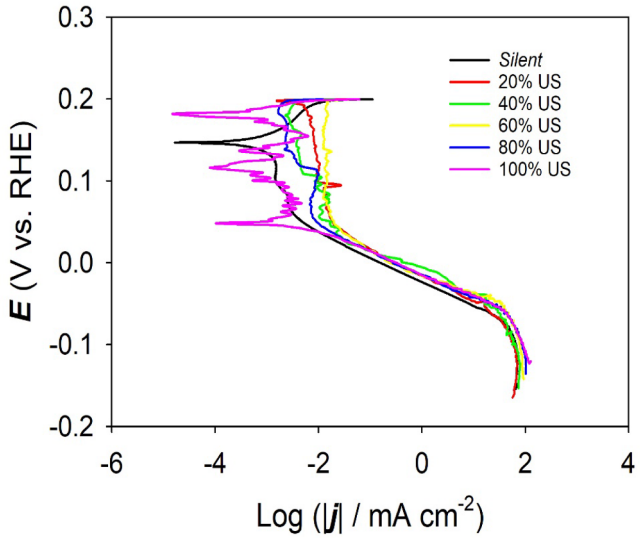

Fig. 6. A series of Tafel plots for the HER occurring at a polycrystalline Pt disc electrode in 0.5 mol/L H_2SO_4 subjected to ultrasound at (a) 0 (*silent*) and (b) 20, 40, 60, 80 and 100% power from LSVs carried out at a scan rate 1 mV/s and at T = 298 K after purging with N_2(g) for 30 min.

electron transfer and improved HER kinetics. However, contrarily to our previous observations, it was found that the A_r was not afftected by the pre-sonicated Pt electrodes, suggesting that other processes might had occurred on the sonicated electrode surface during the sono-LSV experiments. Nonetheless, for a high-performance electrocatalytic process, a low b and a high j_o is required [37] and from this investigation, the best electrochemical conditions were found at 100% ultrasonic amplitude.

3.3. Study of the hydrogen bubbles in the absence and presence of ultrasound

Fig. 7 shows a series of images for the hydrogen evolution on a Pt wire in the absence (Fig. 7(a)) and presence of ultrasound (26 kHz, 100% ultrasonic amplitude - (Fig. 7(b)-(g)) by high-speed imaging. The time between each image was 100 µs. The applied potential was set at −1.30 V vs. RHE with a current of + 80 mA i.e. a current density of + 31.62 mA/cm^2 (316.20 A/m^2). From the figure, it may be observed that under *silent* conditions (Fig. 7(a)), the hydrogen bubbles are very small and similar in size, leaving the Pt wire electrode at a uniform velocity. Some larger hydrogen bubbles were observed which rose faster due probably to buoyancy and drag differences. Under ultrasonic conditions (Fig. 7(b)-(g)), it was found that the hydrogen bubbles formed above the Pt wire electrode agglomerated to form larger hydrogen bubbles possibly due to secondary Bjerknes forces [52] in turn removing small bubbles from the Pt wire surface. Moreover, and interestingly, it was observed that large hydrogen bubbles had uniform sizes and formed well-organised “chains” before forming larger hydrogen bubble clusters. After 0.5 s of continuous sonication, the Pt wire electrode was “cleaned” and a few or even no hydrogen bubbles above the Pt wire electrode were visible as they coalesced with larger ones running along the wire. It was previously found that the collection of pre-existing gas bubbles under sonication are due to 2nd Bjerknes effect which is an expected common effect. Small bubbles easily coalesce to macro-bubbles of larger sizes [33–35,51,52].

From the video (filmed at 10,000 frames per second – see file entitled “USMaxPower(100%).gif [Video Still]”), it can be observed that the hydrogen bubbles seem to migrate to nodes in the electrolyte via the so-called “primary radiation force” [33–35,51]. This effect is known to be due to the difference in the density and compressibility between the gas bubbles as well as the electrolyte phase leading to an “acoustophoretic effect” in which the dispersed bubble migrate to these nodes. When the hydrogen bubble reaches the nodal areas, the secondary Bjerknes force acts between the bubbles to promote coalition [52]. The resulting increase in the size of the bubbles increases their buoyancy augmenting electrolyte hydrogen degassing. It has been previously shown that these processes take place sequentially and simultaneously under sonication [33–35,51]. In our conditions, during the first few microseconds of ultrasonication, the hydrogen bubbles migrate towards the closest pressure nodes, and as they meet nearby bubbles, they hit, coalesce and rise faster to the surface. In other words, under insonation, the hydrogen bubbles detach from the electrode surface when they move from the nucleation site parallel to the electrode surface, they either coalesce with adhering bubbles or collide and are pushed away from the electrode surface.

4. Conclusions

We studied the effects of power ultrasound (26 kHz, up to ~75 W/cm^2) on a platinum (Pt) polycrystalline disc electrode immersed in a 0.5 M H_2SO_4 solution by cyclic and linear sweep voltammetry at 298 K. We observed that, in our experimental conditons, a ~250% increase in current density towards the hydrogen evolution reaction (HER) was achieved at maximum ultrasonic power (100%), although no obvious changes in the “real” surface area (A_r) and roughness factor (R) were observed. It was found that the HER started earlier under sonication at maximum acoustic power i.e. a ΔE shift of ~ + 20 mV was observed, suggesting that ultrasound improves the HER activity on Pt. A nearly 100% increase in the exchange current density (j_o) at 100% ultrasonic amplitude was observed, although the Tafel slopes (b) at high overpotentials were not greatly affected when compared to *silent* conditions. Overall, it was found that ultrasound did not significantly modify the mechanism of HER but instead increased currents at the Pt disc surface area through effective hydrogen bubble removal as indicated by the ultra-fast camera imaging experiments. From this study, it can be

Table 2
Slopes of the LSV branches in the range [−0.05 – −0.10 V vs. RHE], onset potentials (E_{onset}), potentials at −10 mA/cm^2 (E_{-10mA/cm^2}), exchange current densities (j_o) and Tafel slopes (b) at low and high overpotentials under *silent* and ultrasonic conditions (26 kHz) at various acoustic amplitudes (20%, 40%, 60%, 80% and 100%).

Ultrasonic power, P_{acous} W [US amplitude %]	Slopes of the LSV branches mA/cm^2/mV	Onset potentials, E_{onset} mV vs. RHE	Potential at −10 mA/cm^2 E_{-10mA/cm^2} mV vs. RHE	Tafel slope, b at low overpotentials mV/dec	Tafel slope, b at high overpotentials mV/dec	Exchange current density, j_o mA/cm^2
0 (*silent*)	1.15	−17.6	−46	30 ± 2	123 ± 3	0.27 ± 0.07
4.65 [20]	1.28	−11.6	−44	32 ± 2	123 ± 3	0.39 ± 0.07
12.10 [40]	1.20	−7.9	−34	25 ± 4	121 ± 4	0.43 ± 0.11
18.30 [60]	1.27	−7.8	–33	23 ± 5	141 ± 3	0.47 ± 0.05
25.00 [80]	2.11	−7.6	−27	18 ± 6	113 ± 6	0.36 ± 0.03
29.20 [100]	1.93	−5.7	−27	21 ± 4	124 ± 2	0.50 ± 0.19

All measurements have been repeated at least three (3) times.

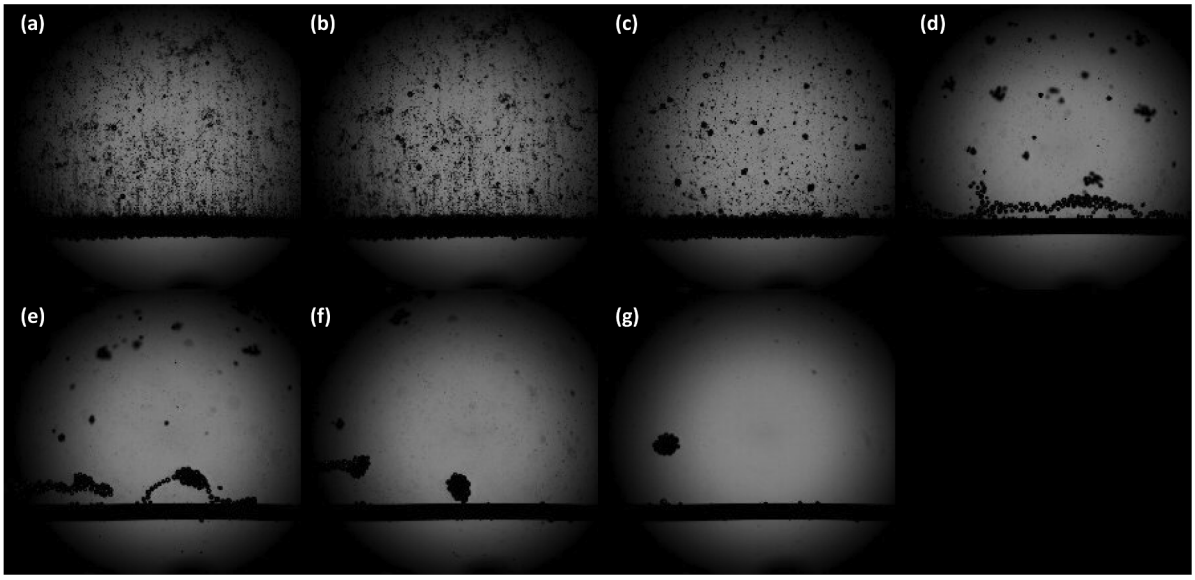

Fig. 7. Hydrogen evolution on a Pt wire in the absence (top left corner) and presence of ultrasound (26 kHz, 100% ultrasonic amplitude). The applied potential was set at −1.30 V vs. RHE – (a) 0 μs, (b) 100 μs , (c) 200 μs, (d) 300 μs, (e) 400 μs, (f) 500 μs, (g) 600 μs. The time between each image is 10^{-4} s (100 μs) filmed at 10,000 frames per second.

postulated that the main contribution of ultrasound is the efficient gas bubble removal from the electrode surface and from the bulk electrolyte in turn reducing the bubble surface coverage and the void fraction of the bulk electrolyte, respectively.

CRediT authorship contribution statement

Bruno G. Pollet: Idea generator, Conceptualization, Supervision, Project management, Writing - review & editing. **Faranak Foroughi:** Experimental, Data analysis, Writing - review & editing. **Alaa Y. Faid:** Data analysis, Writing - review & editing. **David R. Emberson:** Experimental, editing, proof-reading. **Md.H. Islam:** Experimental, Editing.

Declaration of Competing Interest

The authors declare that they have no known competing financial interests or personal relationships that could have appeared to influence the work reported in this paper.

Acknowledgements

The authors would like to thank Prof. Dr. Robert Mettin (Drittes Physikalisches Institut, Georg-August-Universität Göttingen, Germany), Prof. Gregory Jerkiewicz (Queen's University, Chemistry Department, Kingston, Canada) and Prof. Christophe Coutanceau (Catalysis and Non-Conventional Medium group, IC2MP, Université de Poitiers, France) for useful discussions.

Appendix A. Supplementary data

Supplementary data to this article can be found online at https://doi.org/10.1016/j.ultsonch.2020.105238.

References

[1] https://publications.jrc.ec.europa.eu/repository/bitstream/JRC115958/kjna29695enn.pdf – visited on 23 April 2020.
[2] H. Nazir, C. Louis, S. Jose, J. Prakash, N. Muthuswamy, M.E.M. Buan, C. Flox, S. Chavan, X. Shi, P. Kauranen, T. Kallio, G. Maia, K. Tammeveski, N. Lymperopoulos, E. Carcadea, E. Veziroglu, A. Iranzo, A.M. Kannan, Is the H_2 economy realizable in the foreseeable future? Part I: H_2 production methods, Int. J. Hydrogen Energy 45 (27) (2020) 13777–13788.
[3] C. Lamy, C. Coutanceau, S. Baranton, Production of Clean Hydrogen by Electrochemical Reforming of Oxygenated Organic Compounds (Hydrogen and Fuel Cells Primers), 1st Edition. Bruno G. Pollet (Series Editor), Academic Press (2019), ISBN: 978-0-12-821500-5.
[4] C. Coutanceau, S. Baranton, T. Audichon, Hydrogen electrochemical production (Hydrogen and Fuel Cells Primers), 1st Edition. Bruno G. Pollet (Series Editor), Academic Press (2017), ISBN: 978-0-12-811250-2.
[5] D. Bessarabov, P. Millet, PEM water electrolysis (Vol.1) (Hydrogen and Fuel Cells Primers), 1st Edition. Bruno G. Pollet (Series Editor), Academic Press (2018), ISBN: 978-0-12-811145-1.
[6] D. Bessarabov, P. Millet, PEM water electrolysis (Vol.2) (Hydrogen and Fuel Cells Primers), 1st Edition. Bruno G. Pollet (Series Editor), Academic Press (2018), ISBN: 978-0-08-102830-8.
[7] S.S. Kumar, V. Himabindu, Hydrogen production by PEM water electrolysis – a review, Mater. Sci. Energy Technol. 2 (2019) 442–454.
[8] M. Carmo, D.L. Fritz, J. Mergel, D. Stolten, A comprehensive review on PEM water electrolysis, Int. J. Hydrogen Energy 38 (22) (2013) 4901–4934.
[9] K. Zeng, D. Zhang, Recent progress in alkaline water electrolysis for hydrogen production and applications, Prog. Energy Combust. Sci. 36 (3) (2010) 307–326.
[10] S.A. Grigoriev, V.N. Fateev, D.G. Bessarabov, P. Millet, Current status, research trends, and challenges in water electrolysis science and technology, International Journal of Hydrogen Energy, doi: 10.1016/j.ijhydene.2020.03.109.
[11] J. Theerthagiri, E.S.F. Cardoso, G.V. Fortunato, G.A. Casagrande, B. Senthilkumar, J. Madhavan, G. Maia, Highly electroactive Ni pyrophosphate/Pt Catalyst toward hydrogen evolution reaction, ACS Appl. Mater. Interfaces 11 (2019) 4969–4982.
[12] M. Wang, Z. Wang, X. Gong, Z. Guo, The intensification technologies to water electrolysis for hydrogen production – a review, Renew. Sustain. Energy Rev. 29 (2014) 573–588.
[13] A. Angulo, P. van der Linde, H. Gardeniers, M. Modestino, D.F. Rivas, Influence of bubbles on the energy conversion efficiency of electrochemical reactors, Joule 4 (3) (2020) 555–579.
[14] B. Mazza, P. Pedeferri, G. Re, Hydrodynamic instabilities in electrolytic gas evolution, Electrochim. Acta 23 (2) (1978) 87–93.
[15] H. Vogt, The incremental ohmic resistance caused by bubbles adhering to an electrode, J. Appl. Electrochem. 13 (1) (1983) 87–88.
[16] J. Eigeldinger, H. Vogt, The bubble coverage of gas-evolving electrodes in a flowing electrolyte, Electrochim. Acta 45 (2000) 4449–4456.
[17] H. Vogt, R.J. Balzer, The bubble coverage of gas-evolving electrodes in stagnant electrolytes, Electrochim. Acta 50 (10) (2005) 2073–2079.
[18] L.J.J. Janssen, C.W.M.P. Sillen, E. Barendrecht, S.J.D. van Stralen, Bubble behaviour during oxygen and hydrogen evolution at transparent electrodes in KOH solution, Electrochim. Acta 29 (1984) 633–642.
[19] B.G. Pollet, J.-Y. Hihn, M.L. Doche, A. Mandroyan, J.P. Lorimer, T.J. Mason, Transport limited currents close to an ultrasonic horn: equivalent flow velocity determination, J. Electrochem. So. 154 (2007) E131–E138.
[20] B.G. Pollet, A Short Introduction to Sonoelectrochemistry, Electrochem. Soc. Interface Fall 27 (3) (2018) 41–42.
[21] B.G. Pollet (Ed.), Power Ultrasound in Electrochemistry: From Versatile Laboratory Tool to Engineering Solution, John Wiley & Sons, Hoboken, NJ, USA, 2012.
[22] B.G. Pollet, M. Ashokkumar, Introduction to Ultrasound, Sonochemistry and Sonoelectrochemistry, B.G. Pollet, M. Ashokkumar (Eds), SpringerBriefs, Berlin,

Germany, (2019) ISBN: 978-3-030-25862-7.
[23] J. Theerthagiri, J. Madhavan, S.J. Lee, M.Y. Choi, M. Ashokkumar, B.G. Pollet, Sonoelectrochemistry for energy and environmental applications, Ultrason. Sonochem. 63 (2020) 104960.
[24] J. Madhavan, J. Theerthagiri, D. Balaji, S. Sunitha, M.Y. Choi, M. Ashokkumar, Hybrid advanced oxidation processes involving ultrasound: An overview, Molecules 24 (18) (2019) 3341.
[25] M. Lepesant, Sonoelectrochemical production of hydrogen for PEM Fuel Cell applications, Internship Report, ENSICAEN, May 2011, Caen, France.
[26] D. Symes, Sonoelectrochemical (20 kHz) production of hydrogen from aqueous solutions, MRes thesis, University of Birmingham, February 2011, Birmingham, UK. http://etheses.bham.ac.uk/1601/1/Symes11MRes_A1a.pdf.
[27] S.H. Zadeh, MRes thesis, Sonoelectrochemical production of hydrogen via alkaline water electrolysis, University of Birmingham, July 2012, Birmingham, UK.
[28] S.H. Zadeh, Hydrogen production via ultrasound-aided alkaline water electrolysis, J. Automation Control Eng. 2 (2014) 103–109.
[29] M.H. Islam, O.S. Burheim, B.G. Pollet, Sonochemical and sonoelectrochemical production of hydrogen, Ultrason. Sonochem. 51 (2019) 533–555.
[30] S. Banerjee, R. Kumar, K.S. Gandhi, Analysis of ultrasonically enhanced hydrogen evolution for Zn-$NiCl_2$ system, Chem. Eng. Sci. 50 (15) (1995) 2409–2418.
[31] D.J. Walton, L.D. Burke, M.M. Murphy, Sonoelectrochemistry: chlorine, hydrogen, and oxygen evolution at paltinised platinum, Electrochim. Acta 41 (17) (1996) 2747–2756.
[32] H.N. McMurray, D.A. Worsley, B.P. Wilson, Hydrogen evolution and oxygen reduction at a titanium sonotrode, Chem. Commun. 8 (8) (1998) 887–888.
[33] S.D. Li, C.C. Wang, C.C. Chen, Water electrolysis in the presence of an ultrasonic field, Electrochim. Acta 54 (2009) 3877–3883.
[34] J. Li, J. Xue, Z. Tan, Y. Zheng, L. Zhang, Ultrasound-assisted electrolysis in NaOH solution for hydrogen generation, EPD Congress (2011) 919–926.
[35] M.Y. Lin, L.W. Hourng, Ultrasonic wavefield effects on hydrogen production by water electrolysis, J. Chin. Inst. Engineers 37 (2014) 1080–1089.
[36] K. Qian, Z.D. Chen, J.J.J. Chen, Bubble coverage and bubble resistance using cells with horizontal electrode, J. Appl. Electrochem. 28 (1998) 1141–1145.
[37] T. Shinagawa, A.T. Garcia-Esparza, K. Takanabe, Insight on Tafel slopes from a microkinetic analysis of aqueous electrocatalysis for energy conversion, Sci. Rep. 5 (2015) 13801–138022.
[38] J. Theerthagiri, S.J. Lee, A.P. Murthy, J. Madhavan, M.Y. Choi, Fundamental aspects and recent advances in transition metal nitrides as electrocatalysts for hydrogen evolution reaction: A review, Curr. Opin. Solid State Mater. Sci. 24 (1) (2020) 100805.
[39] M.H. Islam, B. Naidji, L. Hallez, A.E. Taouil, J.-Y. Hihn, O.S. Burheim, B.G. Pollet, The use of non-cavitating coupling fluids for intensifying sonoelectrochemical processes, Ultrason. Sonochem. 66 (2020) 10587.
[40] C. Wei, R.R. Rao, J. Peng, B. Huang, I.E.L. Stephens, M. Risch, Z.J. Xu, Y. Shao-Horn, Recommended practices and benchmark activity for hydrogen and oxygen electrocatalysis in water splitting and fuel cells, Adv. Mater. 31 (2019) 1806296.
[41] G. Li, W. Zhou, Carbon-based electrocatalysts for water-splitting. in flexible energy conversion and storage devices, Wiley-VCH Verlag GmbH & Co. KGaA, 2018, 459–483, doi: 10.1002/9783527342631.ch15.
[42] Z. Chen, X. Duan, W. Wei, S. Wang, B.-J. Ni, Recent advances in transition metal-based electrocatalysts for alkaline hydrogen evolution, J. Mater. Chem. A7 (2019) (2019) 14971–15005.
[43] Z.P. Wu, X.F. Lu, S.Q. Zang, X.W. Lou, Non-noble-metal-based electrocatalysts toward the oxygen evolution reaction, Adv. Funct. Mater. 1 (20) (2020) 1910274.
[44] M.A. Margulis, I.M. Margulis, Calorimetric method for measurement of acoustic power absorbed in a volume of a liquid, Ultrason. Sonochem. 10 (2003) 343–345.
[45] F. Contamine, A.M. Wilhelm, J. Berlan, H. Delmas, Power measurement in sonochemistry, Ultrason. Sonochem. 2 (1995) 43–47.
[46] P. Daubinger, J. Kieninger, T. Unmüssig, G.A. Urban, Electrochemical characteristics of nanostructured platinum electrodes – a cyclic voltammetry study, Phys. Chem. Chem. Phys., 16, 2014, 8392–8399.
[47] M. Zeng, Y. Li, Recent advances in heterogeneous electrocatalysts for the hydrogen evolution reaction, J. Mater. Chem. A3 (2015) 14942–14962.
[48] H. Zhang, L.A. Coury, et al., Effects of high-intensity ultrasound on glassy carbon electrodes, Anal. Chem. 65 (1993) 1552–1558.
[49] B.G. Pollet, The Effect of Ultrasound on Electrochemical Parameters, PhD thesis Coventry University, England, UK, 1998.
[50] P.R. Birkin, S. Silva-Martinez, A study of the effect of ultrasound on mass transport to a microelectrode, J. Electroanal. Chem. 416 (1996) 127–138.
[51] N.A. Gumerov, I.S. Akhatov, C.D. Ohl, S.P. Sametov, M.V. Khazimullin, S.R. Gonzalez-Avila, Robust acoustic wave manipulation of bubbly liquids, Appl. Phys. Lett. 108 (13) (2016) 134102–134105.
[52] T.G. Leighton, A.J. Walton, M.J.W. Pickworth, Primary Bjerknes forces, Eur. J. Phys. 11 (1) (1990) 47–49.